EFFECTS OF ENVIRONMENT ON THE SURFACE WAVE CHARACTERISTICS OF A DIELECTRIC-COATED CONDUCTOR—PART IV

GLORY JOHN, R. CHATTERJEE AND S. K. CHATTERJEE

(*Department of E.C.E., Indian Institute of Science, Bangalore* 560012)

Received on May 18, 1976 and in revised form on August 28, 1976

ABSTRACT

The problem of excitation of multilayered-graded-dielectric-coated conductor by a magnetic ring source is formulated in the form of a contour integral which is solved by using the method of steepest descent. Numerical evaluation of launching efficiency shows that high value of about 90 percent can be attained by choosing proper dimensions of the launcher with respect to the dimension of the surface wave line.

Key words: Environmental effect, Surface wave characteristics.

1. INTRODUCTION

Recent investigations [1–4] show that surface wave characteristics of a dielectric-coated conductor are influenced considerably by the dielectric constant, loss tangent and anisotropy of the external medium surrounding the surface wave line. It is also found that surface wave power tends to concentrate more inside the dielectric layers when the center conductor is coated concentrically with two inhomogeneous dielectrics having radial dielectric constant quadratic or fourth-power profiles. Conditions also exist for which surface wave is not supported by the structure.

The object of this paper is to determine the launching efficiency when a multilayered-graded-dielectric-coated conductor is excited by a concentric annular ring. It appears from the work of other authors [5–14] on the excitation of surface waves that the excitation problem for a multilayered-graded-dielectric-coated conductor has not been previously solved.

2. FIELD COMPONENTS

Assuming $\frac{\partial}{\partial \phi} = 0$, the field components (Fig. 1 *a*) are given by

$$E_z = DH_0^{(1)}(ju'\rho)\, e^{j\omega t - \gamma' z}$$

$$E_\rho = D\frac{\gamma}{ju'} H_1^{(1)}(ju'\rho)\, e^{j\omega t - \gamma' z}$$

$$H_\phi = \frac{\omega\epsilon}{u'} DH_1^{(1)}(ju'\rho)\, e^{j\omega t - \gamma' z} \tag{1}$$

which satisfy Maxwell's equations is the space $\rho \geqslant b$, provided

$$(u')^2 = -(\gamma'^2 + k^2) \tag{2}$$

where

$$\gamma' = \alpha + j\beta \text{ and } k^2 = \omega^2 \mu_0 \epsilon_0 \epsilon \tag{2 a}$$

where the principal root is take for u'.

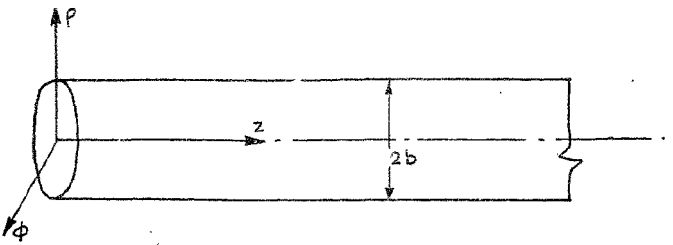

FIG. 1 *a*. Surface Wave Structure—Coordinate System.

In order to excite the surface wave structure, a voltage $Ve^{j\omega t}$ is applied across an infinitesimally narrow slot of radius c, cut in a perfectly conducting screen in the plane $z = 0$ (Fig. 1 *b*). The same field configuration is obtained by a filamentary ring of equivalent magnetic current $2V\delta(\rho - c)\,\delta(z)$, where

$$\delta(z) = \frac{1}{2\pi} \int_{-\infty}^{\infty} e^{-\gamma z}\, d\gamma \tag{3}$$

Hence, the source of excitation consists of the superposed magnetic ring sources of current

$$I_m = \frac{V}{\pi}\, \delta(\rho - c)\, e^{-\gamma z} \tag{4}$$

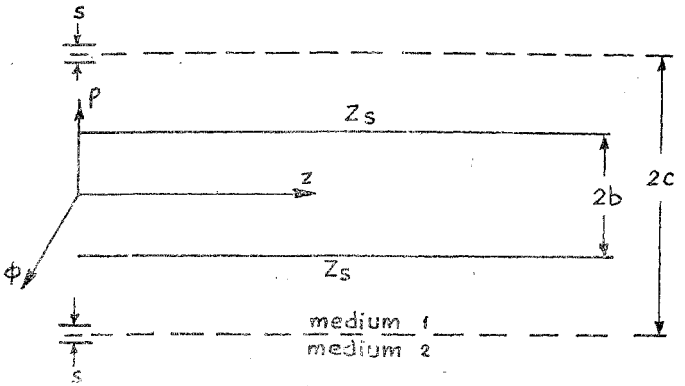

FIG. 1 *b*. Excitation by a Magnetic Ring Source s = slot width, Z_s = surface impedance, b = structure radius, c = slot radius.

The field components in the region $b \leqslant \rho \leqslant c$ are given by

$$E_{z11} = [D_1 H_0^{(1)}(ju\rho) + D_2 H_0^{(2)}(ju\rho)]\, e^{j\omega t-\gamma z}$$

$$E_{\rho 11} = \frac{\gamma}{ju}[D_1 H_1^{(1)}(ju\rho) + D_2 H_1^{(2)}(ju\rho)]\, e^{j\omega t-\gamma z}$$

$$H_{\phi 11} = \frac{\omega\epsilon}{u}[D_1 H_1^{(1)}(ju\rho) + D_2 H_1^{(2)}(ju\rho)]\, e^{j\omega t-\gamma z} \tag{5}$$

which represent standing waves.

The field components in the region $\rho \geqslant c$ are given by

$$E_{z21} = D_3 H_0^{(1)}(ju\rho)\, e^{j\omega t-\gamma z}$$

$$E_{\rho 21} = \frac{\gamma}{ju} D_3 H_1^{(1)}(ju\rho)\, e^{j\omega t-\gamma z}$$

$$H_{\phi 21} = \frac{\omega\epsilon}{u} D_3 H_1^{(1)}(ju\rho)\, e^{j\omega t-\gamma z} \tag{6}$$

which represent

(*a*) outward travelling wave for $u > 0$, imaginary,

(*b*) inward travelling wave for $u < 0$, imaginary, and

(*c*) evanescent wave for $u > 0$, real.

3. Evaluation of Excitation Constants

By applying the conditions of continuity of H_ϕ and discontinuity of E_z by the current density $V/\pi\, e^{-\gamma z}$ across the mangetic current sheet and matching the surface impedance

$$Z_s = \frac{u'}{\omega\epsilon}\frac{H_0^{(1)}(ju'b)}{H_1^{(1)}(ju'b)} = p/\omega\epsilon$$

the excitation constants are obtained as,

where

$$D_1 = \frac{Vcu}{4D^1} H_1^{(1)}(juc);\ D_2 = \frac{Vcu}{4} H_1^{(1)}(juc)$$

$$D_3 = \frac{Vcu}{4D^1}\left[H_1^{(1)}(juc) + D^1 H_1^{(2)}(juc)\right] \tag{7}$$

$$D' = \frac{D_2}{D_1} = \frac{pH_1^{(1)}(jub) - uH_0^{(1)}(jub)}{uH_0^{(2)}(jub) - pH_1^{(2)}(jub)}$$

4. Field Excited by the Annular Slot

Expressing D_1 and D_3 in terms of D', the component $H\phi$ becomes

(i) $b \leqslant \rho \leqslant c$

$$H_{\phi 1} = \frac{V\omega\epsilon c}{4} H_1^{(1)}(juc)\left[\frac{1}{D^1} H_1^{(1)}(ju\rho) + H_1^{(2)}(ju\rho)\right] e^{j\omega t - \gamma z}$$

(ii) $\rho \geqslant c$

$$H_{\phi 2} = \frac{V\omega\epsilon c}{4} H_1^{(1)}(ju\rho)\left[\frac{1}{D^1} H_1^{(1)}(juc) + H_1^{(2)}(juc)\right] e^{j\omega t - \gamma z} \tag{8}$$

Since the functions $H_1^{(1)}(ju\rho)$ and $H_1^{(2)}(ju\rho)$ represent incoming and outgoing waves, the term $1/D'$ can be considered as the reflection coefficient R at the guiding surface.

Thus the field excited by the annular slot of radius c is given by [12]

$$H_{\phi 1} = \frac{V\omega\epsilon c}{4}\int_{-\infty}^{\infty} H_1^{(1)}(juc)\left[H_1^{(2)}(ju\rho) + R_c H_1^{(1)}(ju\rho)\right] e^{-\gamma z}\, d\gamma$$

$$H_{\phi 2} = \frac{V\omega\epsilon c}{4}\int_{-\infty}^{\infty} H_1^{(1)}(ju\rho)\left[H_1^{(2)}(juc) + R_c H_1^{(1)}(juc)\right] e^{-\gamma z}\, d\gamma \tag{9}$$

5. Evaluation of the Infinite Integral

Since u possesses two values $\pm j(k^2+\gamma^2)^{\frac{1}{2}}$ for every value of γ, the integrand in equation (11) is a two-valued function of γ. The integrand is made single-valued by supposing that the set of values of γ belong to two different sheets which have common points at $\gamma = \pm jk$, called the branch points. The branch-cut in the γ-plane divides the u-plane into two parts, each corresponding to one of the γ-sheets. The contour of integration is selected such that it remains on the proper sheet for which Re$u > 0$ which leads to evanescent waves or Im $u < 0$, which leads to outward travelling waves and does not cross the branch-cut which is given by Re $u = 0$. The other sheet of the γ-plane for which Re $u < 0$ is called the improper sheet.

The branch-cut equation Re $u = 0$ leads to $\alpha\beta = k'k''$ which is a portion of a hyperbola (Fig. 2 *a*). As k'' (which accounts for the losses in the medium) decreases the hyperbola (Fig. 2 *b*) becomes a portion of the β-axis ($\gamma = \alpha + j\beta$) between zero and k', and the real axis in the right half-plane. The contour C_γ of the integral must lie entirely in the region Re $u > 0$, Im $u = 0$.

The roots of $1/R_c = 0$, *i.e.*,

$$pH_1^{(1)}(ju'b) - u' H_0^{(1)}(ju'b) = 0 \tag{10}$$

give the surface wave poles which lie on the $j\beta$-axis at distances $\pm(u'^2+k^2)^{\frac{1}{2}}$ from the origin. As the dominant surface wave mode is of importance and the evanescent waves can be ignored at a distance from the launcher, only two poles need to be considered.

For $z > 0$, the contour C_γ (Fig. 3) is represented by

$$C_\gamma = -C_s - C_b - 2\pi j \sum \text{Residues} \tag{11}$$

where C_b and C_s represent respectively contours for the semicircle at infinity and branch-cut integral. Since the integral vanishes on C_s for $z > 0$, the total contributions are from the branch-cut integral (which represents the radiation field with a continuous eigenvalue spectrum) and the residues contributed by the enclosed surface wave poles. In addition to the surface wave poles, there are poles corresponding to the roots of pure Re $u < 0$ and infinite number of leaky wave poles corresponding to complex roots with Re $u < 0$, which lie on the improper sheet.

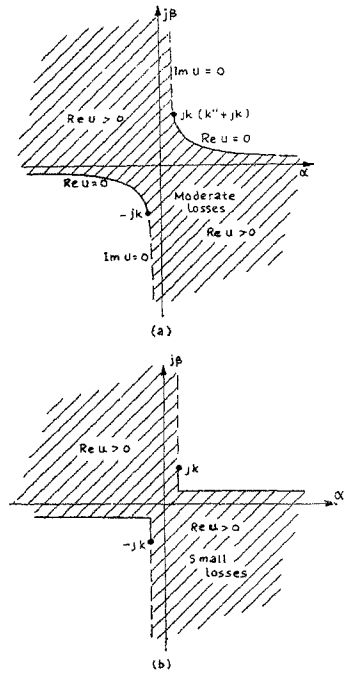

FIG. 2. Branch-cut in the γ-plane.

6. METHOD OF STEEPEST DESCENTS

In order to integrate equation (11), the γ-plane is transferred to ψ-plane by using the transformation $\gamma = jk \cos \psi$ where the complex variable $\psi = \sigma + jn$.

The two sheets of the Riemann surface map into a connected strip of width 2π along the σ-axis (Fig. 4*a*). The condition $\sin\sigma \sinh \eta > 0$ in the ψ plane corresponds to the condition $\operatorname{Re} u > 0$ in the γ-plane. The four quadrants of the γ-plane map into regions designated by T_i and B_i ($i = 1$,

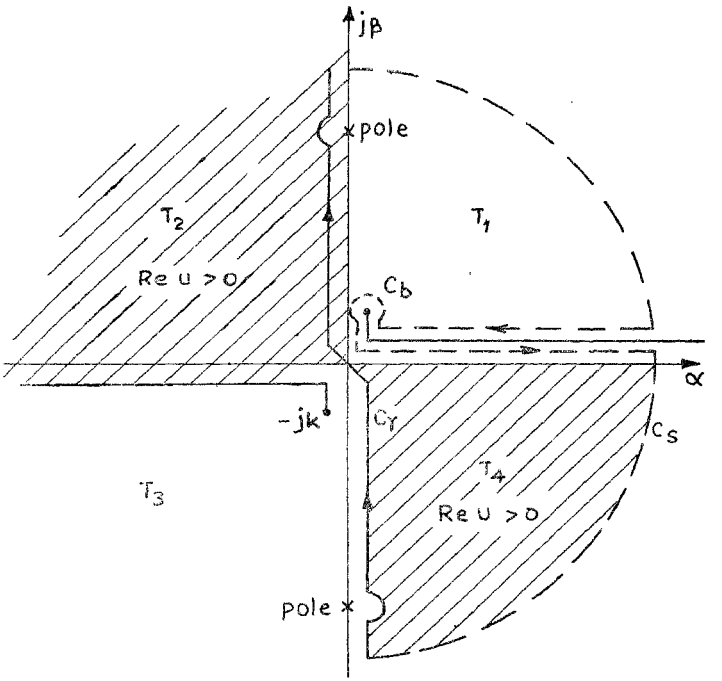

FIG. 3. Branch-cut and the Contour of Integration in the γ-plane.

2, 3, 4) respectively. The hyperbolas giving the branch-cuts in the γ-plane map into the dashed lines. The cross-hatched regions are the corresponding regions in the two figures. The original contour C can be deformed into any convenient contour in the cross-hatched region without changing the value of the integral since no poles will be captured. By using

$$ju = -k \sin \psi,$$

$\alpha+$, $\beta+$ means $\alpha > 0$, $\beta > 0$
$\alpha-$, $\beta-$ means $-\alpha < 0$, $\beta < 0$

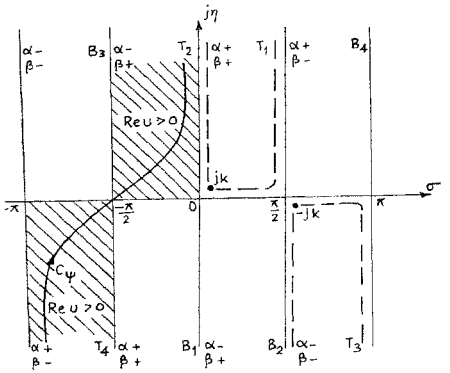

FIG. 4 *a*. Transformation of γ-plane into ψ-plane.

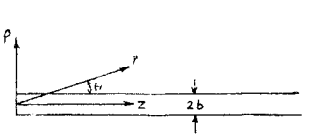

FIG. 4 *b*. Co-ordinate system.

and the coordinate transformation (Fig. 4 *b*) $\rho = r \sin\theta$, $z = r\cos\theta$ and also the asymptotic value for $H_1^{(1)}(k\rho \sin\psi)$, the component $H_{\phi 2}$ becomes

$$H_{\phi 2} = \frac{V\omega\epsilon c}{4} \int_{c_\psi} \left(\frac{2}{\pi kr \sin\theta \sin\psi}\right)^{\frac{1}{2}} \times F(\psi)\, k \sin\psi\, e^{-j\pi/4}\, e^{-jkr\cos(\psi+\theta)}\, d\psi \tag{12}$$

where

$$F(\psi) = H_1^{(2)}(kc \sin\psi) + R_c H_1^{(1)}(kc \sin\psi)$$

$$R_c = -\frac{jk \sin\psi\, H_0^{(2)}(bk \sin\psi) - p\, H_1^{(2)}(bk \sin\psi)}{p\,(H_1^{(1)}(bk \sin\psi) + jk \sin\psi\, H_0^{(1)}(bk \sin\psi)}$$

and

$$p = u' \frac{H_0^{(1)}(ju'b)}{H_1^{(1)}(ju'b)}$$

Using the method of steepest descents, $H_{\phi rad}$ is determined as

$$H_{\phi rad} = \frac{k}{\sqrt{r}} \left(\frac{\pi}{2kr}\right)^{\frac{1}{2}} F(\theta') \times 2e^{-jkr} \tag{13}$$

where

$$F(\theta') = F(-\theta) = H_1^{(2)}(-kc \sin\theta) + R_c\, H_1^{(1)}(-kc \sin\theta)$$

$$R_c = \frac{jk \sin\theta\, H_0^{(2)}(-bk \sin\theta) - p\, H_1^{(2)}(-bk \sin\theta)}{p\, H_1^{(1)}(-bk \sin\theta) - jk \sin\theta\, H_0^{(1)}(-bk \sin\theta)}$$

and

$$K = \frac{V\omega\epsilon c}{4}(2k/\pi)^{\frac{1}{2}}$$

and where the SDC passing through $(-\theta)$ is considered (Figs. 5 *a* and 5 *b*)

In addition to the contribution to the integral from the SDC, there will be contribution from the residues of the surface wave poles which lie on the lines $\sigma = 0$, $\eta > 0$ and $\sigma = \pm\pi$, $\eta < 0$. The leaky wave poles lie on the improper sheet and a finite number of them may be encountered as the contour C is deformed into the section B_1. The surface wave and leaky wave poles contribute only for a range θ greater than some minimum value θ_c, since no poles are crossed for small values of θ, *i.e.*, these poles are not significant in determining the radiation field.

7. Radiated Power

The radiated power P_r is given by

$$P_r = \frac{1}{2} Re \frac{Z_0}{\sqrt{\epsilon}} \int_{\theta=0}^{\pi/2} \int_{\psi=0}^{2\pi} |H_{\phi rad}|^2 r^2 \sin\theta\, d\theta\, d\psi \tag{14}$$

which reduces to

$$P_r = \frac{Z_0}{\sqrt{\epsilon}} \frac{\pi}{\epsilon} \left(\frac{Vc\omega\epsilon}{2}\right)^2 \int_{\theta=0}^{\pi/2} F(\theta')^2 \sin\theta\, d\theta \tag{15}$$

where Z_0 is the free space impedance.

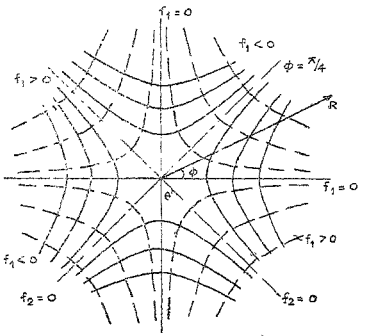

FIG. 5 *a*. Plots of f_1 and f_2 in the R-ϕ plane.

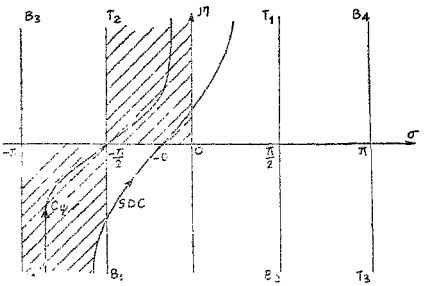

FIG. 5 *b*. Steepest Descent Contour in the ψ-plane.

8. EVALUATION OF THE SURFACE WAVE FIELD

The surface wave field is given by the residue of the poles of the integrand

$$[H_1^{(2)}(juc) + R_c H_1^{(1)}(juc)] H_1^{(1)}(ju\rho) e^{-\gamma z}$$

The poles are given by

$$u H_0^{(2)}(jub) - p H_1^{(2)}(jub) = 0 \tag{16}$$

which has the root $u = u'$. The residue at the pole $u = u'$ is given by

$$\text{Res} = -\frac{2ju'}{b\gamma'} \frac{K_1(u'c)}{f(u'b)} \left(-\frac{2}{\pi}\right) K_1(u'\rho)\, e^{-\gamma' z} \tag{17}$$

where

$$f(u'b) = K_0^2(u'b) - K_1^2(u'b) + \frac{2}{u'b} K_0(u'b) K_1(u'b) \tag{17a}$$

The magnetic field component of the surface wave is given by

$$H_{\phi s} = 2V\omega\epsilon \left(\frac{c}{b}\right) \left(\frac{u'}{\gamma'}\right) \frac{K_1(u'c) K_1(u'\rho)}{(u'b) f(u'b)} e^{-\gamma' z} \tag{18}$$

The electric field component is given by

$$E_{\rho s} = Z_\omega H_{\phi s} \tag{19}$$

where,

$Z_w = -j\sigma'/\omega\epsilon$ represents the wave impedance of the surface wave.

The total power carried by the surface wave is

$$P_s = \int_{\phi=0}^{2\pi} \int_{\rho=b}^{\infty} \tfrac{1}{2}\, Re\, [E_{\rho s} H_{\phi s}^*]\, \rho\, d\rho\, d\phi$$

$$= 2\pi V^2 \frac{\omega\epsilon}{\beta} (c/b)^2 \frac{K_1^2(u'c)}{f(u'b)} \tag{20}$$

9. Launching Efficiency

The launching efficiency defined by

$$\eta_e = \frac{P_s}{P_s + P_r}$$

gives, on evaluation,

$$\eta_e = \left[\frac{2}{\beta b^2} \frac{K_1^2(u'c)}{b(u'b)}\right] \Big/ \left[\frac{2}{b^2\beta} \frac{K_1^2(u'c)}{f(u'b)} + k \cdot I\right] \tag{21}$$

where

$$I = \int_{\theta=0}^{\pi/2} \frac{[R_1 J_1(cq) - I_1 Y_1(cq)]^2}{R_1^2 + I_1^2} \sin\theta\, d\theta$$

$$R_1 = q\, Y_0(bq) + u' \frac{K_0(u'b)}{K_1(u'b)}\, Y_1(bq)$$

$$I_1 = q\, J_0(bq) + u' \frac{K_0(u'b)}{K_1(u'b)}\, J_1(bq)$$

$q = k \sin\theta.$

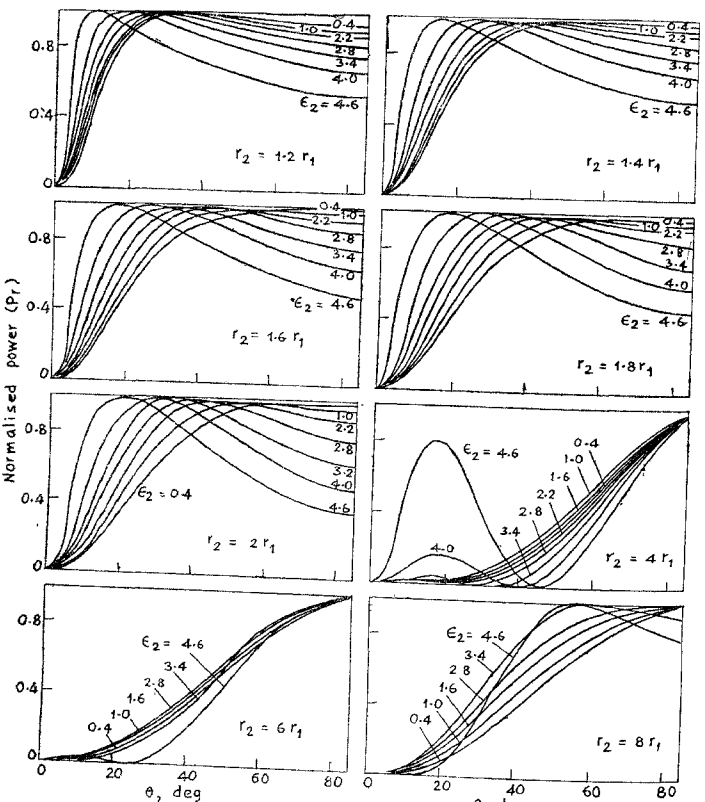

FIG. 6. Radiation plots for the source-excited field $r_1 = 0{\cdot}1$ cm, $b = r_2$, $c = 2\,b$, $\epsilon_1 = 5{\cdot}0$. (Figures 6 to 12 are for the case of a dielectric-coated conductor in isotropic medium.)

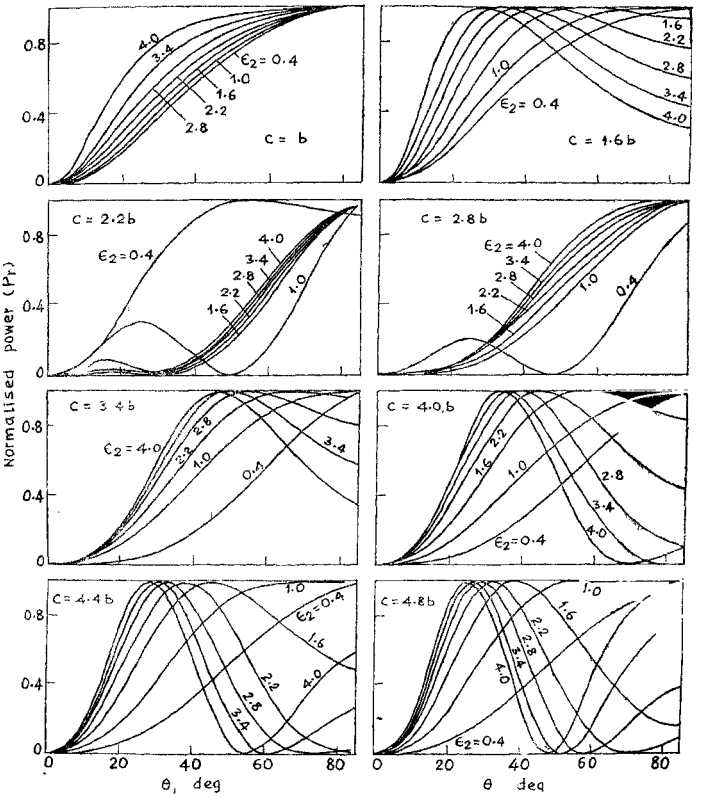

FIG. 7. Radiation plots for the source-excited field $r_1 = 0{\cdot}2$ cm, $b = r_2 = 0{\cdot}4$ cm, $\epsilon_1 = 5{\cdot}0$.

For the case of an inhomogeneous dielectric the inhomogeneity factor appears while determining the root u' [4].

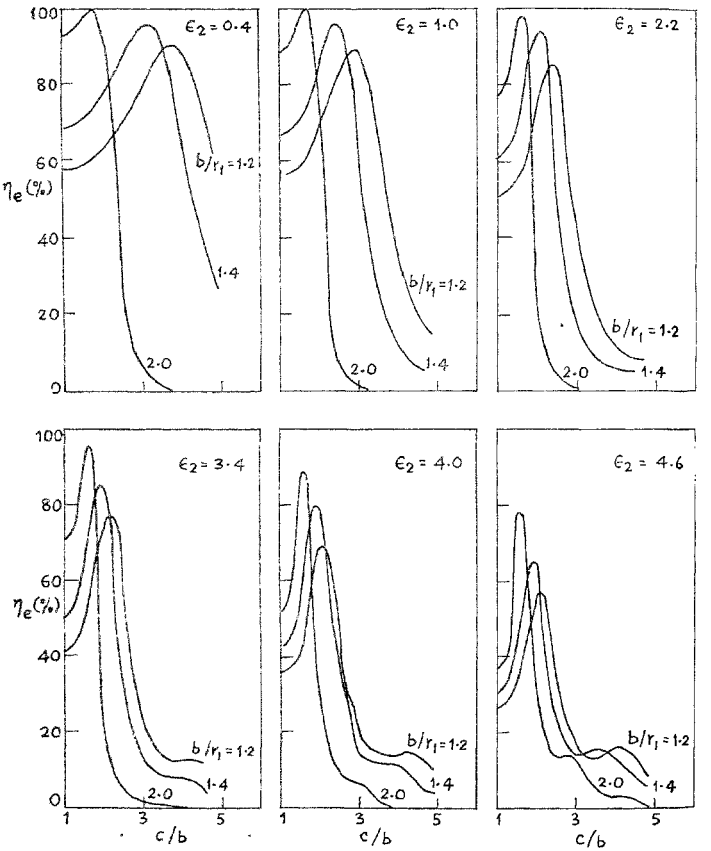

FIG 8. Plots of launching efficiency $r_1 = 0.3$ cm, $b = r_2$, $\epsilon_1 = 5.0$.

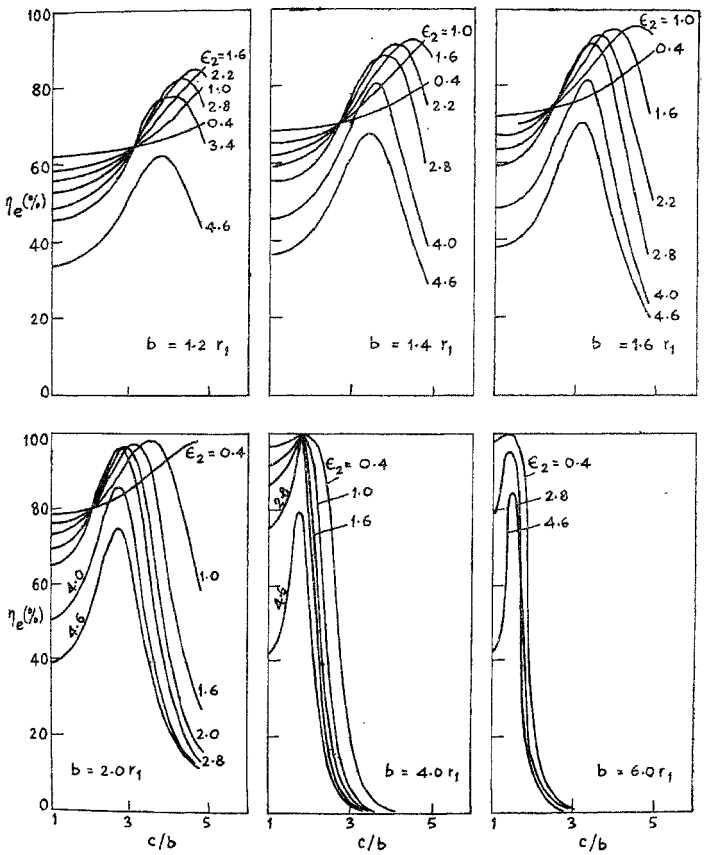

FIG 9. Plots of launching efficiency. $r_1 = 0{\cdot}1$ cm, $b = r_2$, $\epsilon_1 = 5{\cdot}0$.

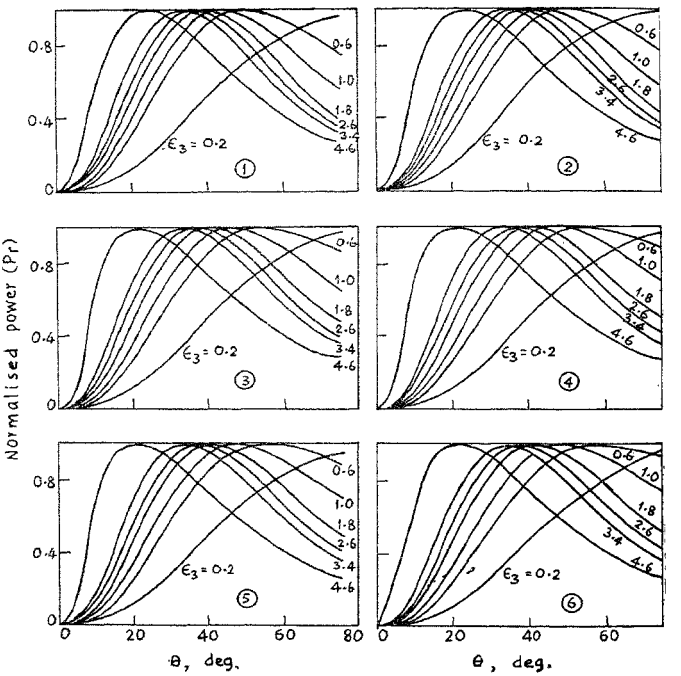

FIG. 10. Radiation plots for the source-excited field. $r_1 = 0{\cdot}1$ cm, $r_\rho = 0{\cdot}12$ cm, $b = r_2 = 0{\cdot}62$ cm, $\epsilon_1 = 5{\cdot}0$, $d = 0{\cdot}4$ cm^{-2}, $c = 1{\cdot}4\,b$.

[Figures 10 and 11 are for the case of a dielectric-coated conductor coated with a graded dielectric—in isotropic medium. The profiles (1)–(6) are given by

(1) $\epsilon_2(\rho) = \epsilon_1 [1 - d^4 (\rho - r_2)^4]$

(2) $\epsilon_2(\rho) = \epsilon_1 \operatorname{sech} d(\rho - r_2)$

(3) $\epsilon_2(\rho) = \epsilon_1 \operatorname{sech}^2 d(\rho - r_2)$

(4) $\epsilon_2(\rho) = \epsilon_1 [1 - d^2 (\rho - r_2)^2]$

(5) $\epsilon_2(\rho) = \epsilon_1 [1 - d^2 (\rho - r_2)^2 - d^4 (\rho - r_2)^4]$

(6) $\epsilon_2(\rho) = \epsilon_2 = 4{\cdot}8$].

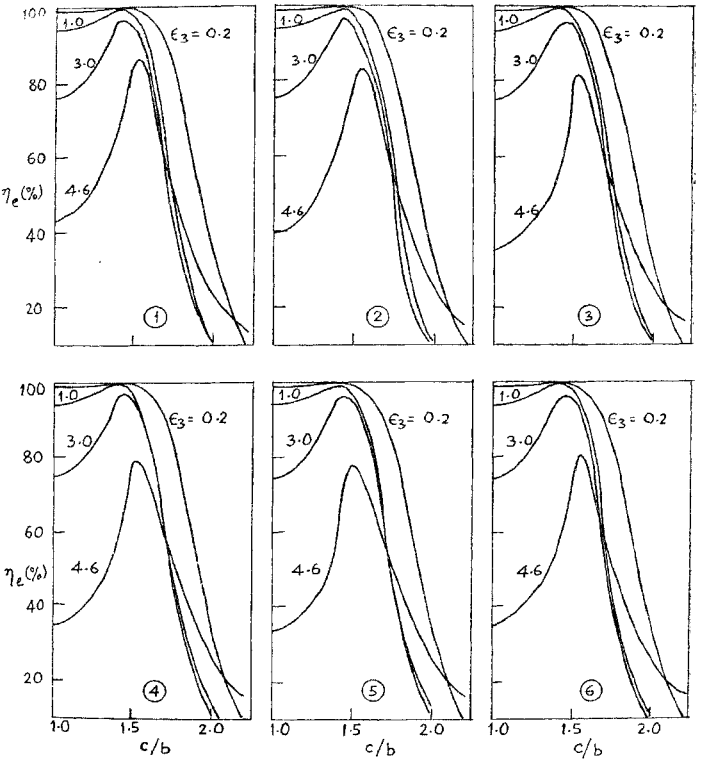

FIG. 11. Plots of launching efficiency for the graded rods. $r_1 = 0{\cdot}1$ cm, $r_2 = 0{\cdot}12$ cm, $b = r_3 = 0{\cdot}62$ cm, $\epsilon_1 = 5{\cdot}0$.

10. NUMERICAL RESULTS

Numerically computed values of radiated power, launching efficiency as function of different parameters, using as function of different parameters, using the IBM/360/44 digital computer are presented graphically in Figs. 6–13.

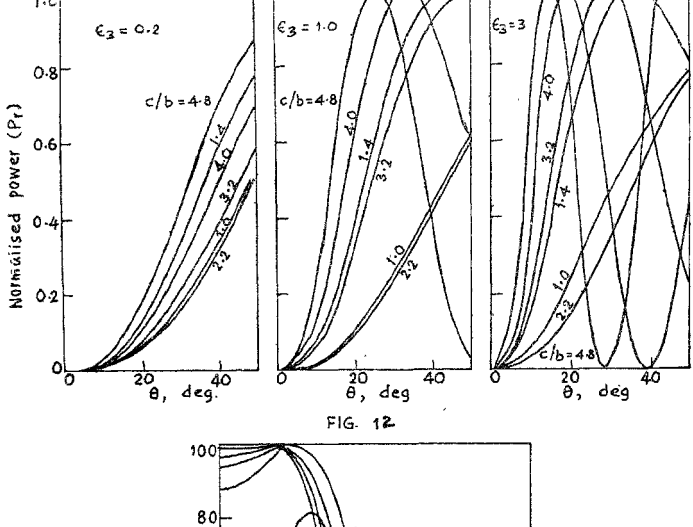

FIG. 12

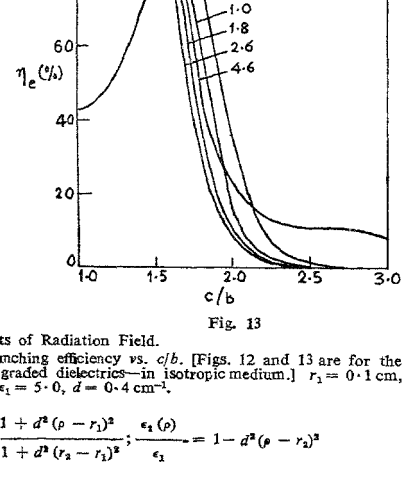

Fig. 13

FIG. 12. Plots of Radiation Field.

FIG. 13. Launching efficiency *vs.* c/b. [Figs. 12 and 13 are for the case of a conductor coated with two graded dielectrics—in isotropic medium.] $r_1 = 0{\cdot}1$ cm, $r_2 = 0{\cdot}12$ cm, $r_3 = 0{\cdot}62$ cm, $b = r_3$, $\epsilon_1 = 5{\cdot}0$, $d = 0{\cdot}4$ cm^{-1}.

Profiles:

$$\frac{\epsilon_1(\rho)}{\epsilon_1} = \frac{1 + d^2(\rho - r_1)^2}{1 + d^2(r_2 - r_1)^2}; \quad \frac{\epsilon_1(\rho)}{\epsilon_1} = 1 - d^2(\rho - r_2)^2$$

11. General Discussions and Conclusions

The surface wave characteristics of Harms-Goubau line are well established. The investigations [1-4] show that if the loss tangent tan δ_2 of the external medium is greater than the loss tangent tan δ_1 of the dielectric coating of the *H*-G line, the imaginary part b_2 of the radial propagation constant u_2 becomes negative, leading to a radially outward power flow which may be interpretted as loss of power by transformation of surface wave power to radiated power. This leads to the conclusion that for long distance communication in which case the surface wave line may have to be buried inside the earth or submerged in ocean, the surface wave line consisting of a conductor coated with a low loss dielectric is not suitable as tan δ for a typical marshy soil is about 0·29 and for sea water it is about 0·6, whereas, for a low loss dielectric coating it is of the order of 0·0005.

The results of the investigations [1–4] including the present report show that

(i) For a homogeneous dielectric-coated conductor coated concentrically with another inhomogeneous dielectric, *Re* (u) is almost same as that of Harms-Goubau line.

(ii) For a conductor coated concentrically with two inhomogeneous dielectrics, radial field decay is not very much different from the above case.

(iii) In the case of a surface wave line immersed in an anisotropic dielectric medium, rate of radial field decay increases with increase of anisotropy factor $s = \epsilon_z/\epsilon_\rho$ increase being more in the case of a conductor coated with inhomogeneous dielectrics.

(iv) Rate of radial field decay is significantly influenced by ϵ_ρ and s. The rate of decay is more as s increases up to a certain value of ϵ_ρ, thereafter the rate of decay decreases as ϵ_ρ increases further, which is due to the effect of ϵ_ρ on the nature of decay coefficient. The value of the ratio of $t =$ tan δ /tan δ_σ does not, however, influence appreciably the rate of radial field decay. A comparative study is shown in Figs. 14 and 15.

(v) Division of power flow in different cases show increased concentration of power inside dielectric layers in the case of a conductor coated with two inhomogeneous dielectrics, the concentration of power being the greatest for quadratic and fourth power profiles of diclectric constant in the radial direction.

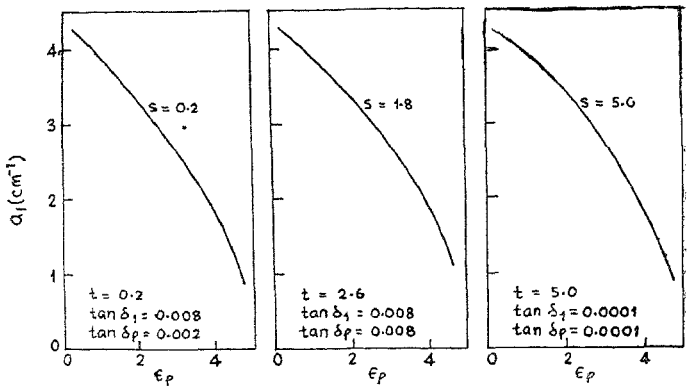

FIG. 14. Variation of a_1 with ϵ_ρ.

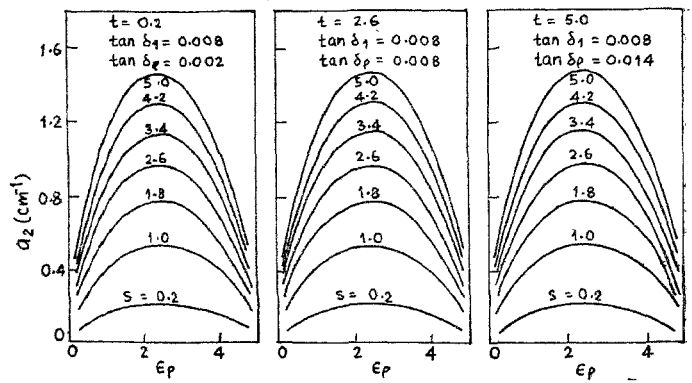

FIG. 15. Variation of a_2 with ϵ_ρ. $r_1 = 0{\cdot}1$ cm, $r_2 = 0{\cdot}12$ cm, $\epsilon_1 = 5{\cdot}0$, $s = \epsilon_2/\epsilon_\rho$, $t = \tan\delta_2/\tan\delta_\rho$.

A comparative study of different cases are presented in Fig. 16 and Table 1.

(vi) Attenuation of surface wave power flow is mainly due to ohmic-loss in the conductor and also due to comparatively lower loss in the dielec-

TABLE I

Division of Power Flow in Different Media (As percentage of total power flow) $r_1 = 0{\cdot}1\,\text{cm}$, $r_2 = 0{\cdot}12\,\text{cm}$, $r_3 = 0{\cdot}62\,\text{cm}$, $\epsilon_1 = 5{\cdot}0$, $\epsilon_\rho = 3{\cdot}0$, $s = \epsilon_z/\epsilon_\rho$, $\epsilon_3 = 3{\cdot}0$

Nature of the Structure	P_z (%)		
	I Medium (Dielectric)	II Medium (Dielectric)	III Medium (Outside)
1. Conductor coated with two inhomogeneous (fourth power profiles) dielectrics; external medium is homogeneous and isotropic	0·005	89·126	10·869
2. Conductor coated with two dielectrics, the outer one being inhomogeneous (quadratic profile); external medium is homogeneous and isotropic	10·120	78·685	11·195
3. Conductor coated with two homogeneous dielectrics ($\epsilon_2 = 4{\cdot}8$); external medium is homogeneous and isotropic	10·006	79·535	10·459
4. Goubau line (case 2 or 3 without the the second coating); external medium is homogeneous and isotropic	4·32	..	95·68
4*a*. Goubau line with coating thickness equal to the overall coating thickness of the cases 1, 2 and 3; external medium is homogeneous and isotropic	90·298	..	9·712
5. Case 1 (with quadratic profile); external medium is anisotropic ($s = 2{\cdot}6$)	0·004	89·412	10·584
6. Base 2 (with fourth power profile) external medium is anisotropic ($s = 3{\cdot}4$)	10·323	81·986	7·691
7. Case 3 with anisotropic external medium ($s = 1{\cdot}8$)	9·966	80·823	9·211
8. Case 4 with anisotropic external medium ($s = 4{\cdot}2$)	6·150	..	93·850
8*a*. Case 4*a* with anisotropic external medium ($s = 5{\cdot}0$)	93·302	..	6·698

tric coating. The overall attenuation is less in the case when both the dielectric coatings are inhomogeneous. Figure 17 shows a comparison of the attenuation constant α for different cases.

(vii) Launching efficiency tends to attain a maximum value for an optimum value of the ratio of the slot radius to the overall radius of the dielec-

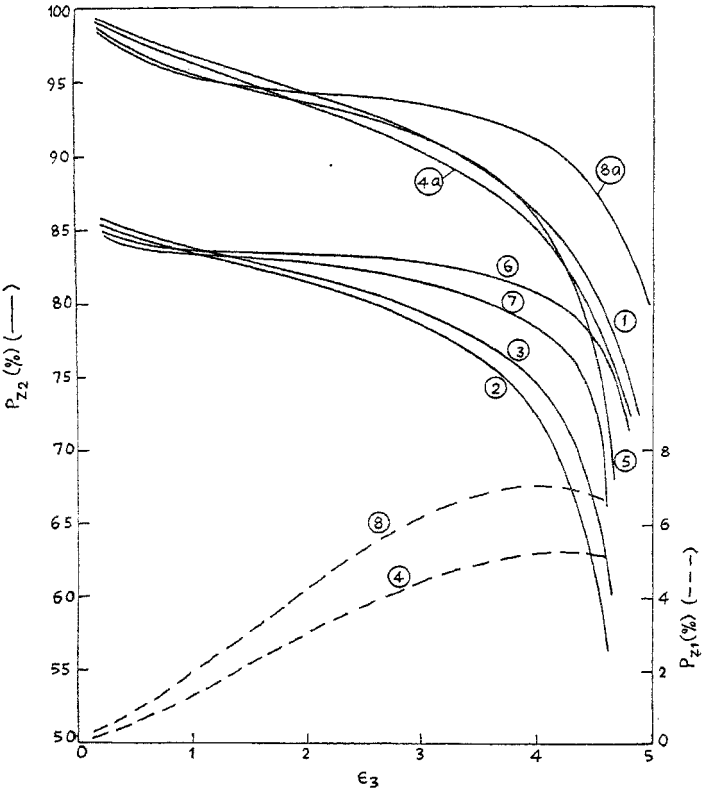

FIG. 16. Comparison of power flow. $r_1 = 0{\cdot}1$ cm, $r_2 = 0{\cdot}12$ cm, $r_3 = 0{\cdot}62$ cm, $\epsilon_1 = 5{\cdot}0$, $d = 0{\cdot}2$ cm^{-1}.

[The different cases (1) to (8 *a*) are as given in Table 1, with $s = 3{\cdot}4$ in (5), $s = 5{\cdot}0$ in (6) $s = 2{\cdot}6$ in (7), $s = 4{\cdot}2$ in (8) and $s = 5{\cdot}0$ in (8 *a*).]

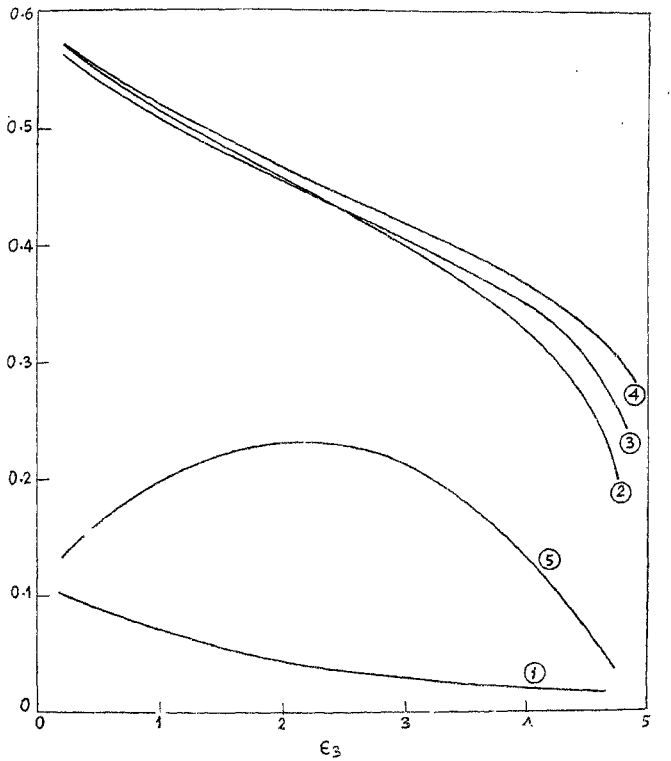

FIG. 17. Comparison of attenuation constants, $r_1 = 0{\cdot}1$ cm, $r_2 = 0{\cdot}12$ cm, $r_3 = 0{\cdot}62$ cm, $\epsilon_r = 5{\cdot}0$, $d = 0{\cdot}2$ cm^{-1}.

(1) Conductor coated with two graded dielectrics.

(2) Dielectric-coated conductor coated with a graded dielectric.

(3) Conductor coated with two homogeneous dielectrics.

(4) Goubau line [cases (2) and (3) without 2nd coating].

(5) Goubau line [coating thickness equal to $r_3 - r_2$ of cases (1) to (3)].

tric-coated line. So, most of the input power can be transformed to surface wave power by a proper design of the launcher with respect to the radial dimension of the surface wave structure.

As a result of the present series of investigations with reference to the possibility of long distance communication of microwave power by cable, it may be concluded that further work is necessary regarding proper choice of dielectric profiles and their distributions, and development of lower loss dielectric, before a multilayered dielectric-coated cable can be utilised for transporting intelligence at super-high frequencies.

REFERENCES

[1] Glory John, Chatterjee, R. and Chatterjee, S. K. — Surface wave characteristics of a lossy dielectric-coated conductor immersed in a lossy dielectric medium, *Proc. I.E.R.E. (India)*, 1974, **12**, 210–227.

[2] Glory John and Chatterjee, S. K. — Effects of environment on the surface wave characteristic of a dielectric-coated conductor—Part I, *Jour. Ind. Inst. Sci.*, 1974, **56**, 88–103.

[3] Glory John, Chatterjee, R. and Chatterjee, S. K. — Effects of environment on the surface wave characteristics of a dielectric-coated conductor—Part II, *Jour. Ind. Inst. Sci.*, 1975, **57**, 113–126.

[4] Glory John, Chatterjee, R. and Chatterjee, S. K. — Effects of environment on the surface wave characteristics of a Dielectric-Coated Conductor—Part III, *Jour. Ind. Inst. Sci.*, 1976, **58**, 123–174.

[5] Cullen, A. L. .. The excitation of plane surface waves, *Proc. IEE (London)*, 1954, **101**, 225–234.

[6] Cullen, A. L. .. A note on the excitation of surface waves, *Proc. IEE (London)*, 1957, **104**, Part C, 472–474.

[7] Fernando, W. M. G. and Barlow, H. E. M. — An investigation of the properties of radial cylindrical surface waves launched over flat reactive surfaces, *Proc. IEE (London)*, 1956, **103**, Part B, 307–318.

[8] Brown, J. and Sharma, K. P. — The launching of radial cylindrical surface waves by a circumferential slot, *Proc. IEEE (London)*, 1959, **106**, Part B, 123–128.

[9] Duncan, J. W. .. The efficiency of excitation of a surface wave on a dielectric cylinder, *IRE Trans. on Micr. Th. Tech.*, 1959, *MTT*-7, 258–267.

[10] Wait, J. R. .. Excitation of surface waves on conducting, stratified dielectriclad and corrugated surfaces, *J. Res. Natl. Bur. Stand.*, 1957, **59**, 365–377.

[11] Brown, J. and Stachera, H. S. — Annular slot launchers for single conductor transmission lines, *Proc. IEE (London)*, 1959, **106**, Part B, Supplement No. 13, 143–145.

[12] Brown, J. and Stachera, H. S. The launching of an axial cylindrical surface wave, *Proc. IEE (London)*, 1962, **109**, Part C, 18–25.

[13] Collin, R. E. .. *Field Theory of Guided Waves*, McGraw-Hill Book Co., Inc., New York, N.Y.

[14] Girija, H. M. and Chatterjee, S. K. Theoretical study of the Farfield of corrugated circular metal rod excited in Eo-mode, *Ind. J. Pure and Appl. Phys.*, 1972, **10**, 794–802.